

Multiplicative Noise and Blur Removal by Framelet Decomposition and l_1 -Based L-Curve Method

Fan Wang, Xi-Le Zhao, and Michael K. Ng

Abstract—This paper proposes a framelet-based convex optimization model for multiplicative noise and blur removal problem. The main idea is to employ framelet expansion to represent the original image and use the variable decomposition to solve the problem. Because of the nature of multiplicative noise, we decompose the observed data into the original image variable and the noise variable to obtain the resulting model. The original image variable is represented by framelet, and it is determined by using l_1 -norm in the selection and shrinkage of framelet coefficients. The noise variable is measured by using the mean and the variance of the underlying probability distribution. This framelet setting can be applied to analysis, synthesis, and balanced approaches, and the resulting optimization models are convex, such that they can be solved very efficiently by the alternating direction of a multiplier method. An another contribution of this paper is to propose to select the regularization parameter by using the l_1 -based L-curve method for these framelet based models. Numerical examples are presented to illustrate the effectiveness of these models and show that the performance of the proposed method is better than that by the existing methods.

Index Terms—Multiplicative noise, blur removal, framelet, convex optimization, sparsity.

I. INTRODUCTION

IN THIS paper, we study blur removal and multiplicative noise degradation in image restoration problems (see [1], [3], [4], [9], [10]). The model of the degradation process is given by

$$g = Af \circ n, \quad (1)$$

Manuscript received September 10, 2015; revised February 8, 2016 and May 11, 2016; accepted June 11, 2016. Date of publication June 22, 2016; date of current version July 21, 2016. This work was supported in part by the Hong Kong Baptist University through the Faculty Research under Grant FRG2/14-15/087 and in part by the Research Grants Council through the General Research Fund under Grant 202013, Grant 12301214, and Grant 13056216. The work of F. Wang was supported by the National Natural Science Foundation of China (NSFC) under Grant 11301239 and Grant 11571156. The work of X.-L. Zhao was supported in part by the 973 Program under Grant 2013CB329404 and in part by NSFC under Grant 61370147 and Grant 61402082. The associate editor coordinating the review of this manuscript and approving it for publication was Prof. Gene Cheung. (*Corresponding author: Michael K. Ng.*)

F. Wang is with the Department of Mathematical and Statistics, Lanzhou University, Lanzhou 730000, China (e-mail: fanwang@lzu.edu.cn).

X.-L. Zhao is with the School of Mathematical Sciences, University of Electronic Science and Technology of China, Chengdu 610051, China (e-mail: xlzhao122003@163.com).

M. K. Ng is with the Centre for Mathematical Imaging and Vision, Department of Mathematics, Hong Kong Baptist University, Hong Kong (e-mail: mng@math.hkbu.edu.hk).

Color versions of one or more of the figures in this paper are available online at <http://ieeexplore.ieee.org>.

Digital Object Identifier 10.1109/TIP.2016.2583793

where A is a spatial-invariant blurring matrix, f is an original image n is a noise vector, and g is the observed image. Here \circ refers to the component-wise multiplication. Note that the noise can follow Gaussian distribution, Gamma distribution or Rayleigh distribution [18]. In synthetic aperture radar images [1], [11], Gamma multiplicative noise removal is considered and A is equal to the identity matrix (without blurring). In ultrasound imaging [12], Rayleigh multiplicative noise removal is studied. Moreover, the degradation by blur and multiplicative noise occurs in many optical coherent imaging systems [5]. For example, when we deal with nonlinear image restoration problems [6], the transformed problem involves both blur and multiplicative noise removal.

In the literature, Rudin *et al.* [9] derived the first multiplicative noise removal method based on the total variation regularization and the variance of noise. Aubert and Aujol [1] designed a numerical method by using Maximum a Posteriori (MAP) estimation approach. Shi and Osher [10] proposed to consider a noisy observation $\log g = \log f + \log n$ and derived the total variation minimization model for multiplicative noise removal problems. Huang *et al.* [3] also used the logarithm transformation $f = \exp(f')$ and considered the total variation regularization for f' in their model (EXP model). Durand *et al.* [2] also used the log-image data and applied a hard-thresholding on the curvelet transform of g ; then they studied of an l_1 data-fidelity term of the thresholded curvelet coefficients and a total variation regularization term in the log-image domain to obtain the denoised image. Dictionary learning methods [13] and nonlocal mean methods [14] are also proposed and developed for multiplicative noise removal, see [13]. Spatial-varying parameters regularization is developed for multiplicative noise removal problems [4].

The methods given in [1] and [9] can be extended to deal with the blur and multiplicative noise removal. Both methods can be very slow and the cost can be very expensive since gradient projection methods are applied to solving these models. Huang *et al.* [15] studied an optimization method to handle both blur and multiplicative noise removal by adding a Gaussian noise penalty term in the model. In [16], Wang and Ng studied a constrained TV-regularized image restoration model on log-image domain, approximated a set of nonconvex constraints by a set of convex constraints, and then applied the alternating direction of multipliers method to solve the resulting optimization problem. Dong and Zeng [17] proposed a convex relaxation models consisting of a MAP estimator based on Gamma noise, a quadratic term and the TV regularization. The quadratic term is based on the statistical property of the Gamma noise only. Recently, Zhao *et al.* [18] studied a convex

optimization model for blur and multiplicative noise removal by using variable decomposition in (1) as follows:

$$Af - g \circ z = 0, \quad (2)$$

where z is a vector where its entry is equal to the reciprocal of the entry of n . In the model, Zhao *et al.* [18] considered to determine f such that $Af - g \circ z$ is close to zero measured in ℓ_1 -norm and the total variational regularization term is small.

In this paper, we make use of framelet expansion to represent the original image so that the difference between $g \circ z$ and Af can be further reduced, can be measured more effectively by using ℓ_1 -norm. More precisely, we propose the following optimization model for multiplicative noise and blur removal problem:

$$\min_{z, f} \|g \circ z - Af\|_1 + \alpha \|Df\|_1 \text{ subject to } \|z - \mu e\|_2^2 \leq \gamma \quad (3)$$

where α is a positive regularization number to control the balance between the data-fitting term and the regularization term of framelet coefficients in the objective function, γ is given such that the variance of noise is small enough, μ can be set to be the mean value of z , e is a vector of all ones, D is the analysis operator in a framelet expansion, and $\|\cdot\|_1$ is the ℓ_1 -norm of a vector. We remark that the proposed approach is different from [18]. The total variation regularization model is used in [18], and this model regularizes restored images with edges recovery. The proposed model employs framelet expansion for blur and multiplicative noise removal. The sparse representation of framelet expansion can provide good image restoration results. This framelet setting can be applied to analysis, synthesis and balanced approaches, see [19]–[23]. Our numerical examples will be shown that the performance of the proposed method is better than that in [18].

On the other hand, we also propose to employ the idea of L-curve [32]–[35] by considering the points generated by the two terms: $\|g \circ z - Af\|_1$ and $\alpha \|Df\|_1$ (corresponding to the (3)), and determine the regularization parameter α based on them. This approach enables us to find a suitable value of α automatically and achieve the balance between the data-fitting term and the regularization term objectively. It is interesting to note in [32] and [33] that the L-curve method is traditionally based on ℓ_2 -norm. The use of ℓ_1 -norm in the L-curve is different from [32] and [33]. We will present experimental results to show the proposed method is quite efficient and it can provide a good quality of recovered images under the degradation of multiplicative noise and blur.

The rest of this paper is organized as follows. In Section 2, we give some preliminaries and present the tight-frame expansion used in our model. In Section 3, we develop the numerical method for solving it. In Section 4, experimental results are reported to demonstrate the effectiveness of the proposed model and the efficiency of the proposed numerical scheme. Finally, some concluding remarks are given in Section 5.

II. TIGHT-FRAME EXPANSION

In this section, we briefly introduce the basics of tight-frame expansion used in [19]–[23] which are based on

tight-frame transformations. All tight-frame transformation D have an important property: $D^T D = I$, here I is the identity transformation. Unlike the orthonormal case, we emphasize that $DD^T \neq I$ see [24]. The matrix D is called the analysis (or decomposition) operator, and its adjoint D^T is called the synthesis (or reconstruction) operator. In order to apply the the tight-frame algorithm, filtering coefficients are used. For example, the filter coefficients for piecewise linear B-spline [24] are given as follows:

$$h_0 = \frac{1}{4}[1, 2, 1], \quad h_1 = \frac{\sqrt{2}}{4}[1, 0, 1], \quad h_2 = \frac{1}{4}[-1, 2, -1]. \quad (4)$$

The tight-frame coefficients of any given vector v corresponding to filter h_i can be obtained by convolving h_i with v . For each filter, we can construct its corresponding filter matrix which is just the circulant matrix with diagonals given by the filter coefficients, such as $H_0 = \frac{1}{4}\text{tridiag}[1, 2, 1]$. Then the one-dimensional tight-frame forward transformation is given by

$$D = \begin{bmatrix} H_0 \\ H_1 \\ H_2 \end{bmatrix} \quad (5)$$

To apply the tight-frame transformation onto v is equivalent to computing Dv , and $H_i v$ gives the tight-frame coefficients corresponding to the filter h_i . The high dimensional piecewise linear B-spline tight-frame is constructed by using tensor products of D , see for instance [25]. For example, the tight-frame coefficients with respect to $h_{i,j} = h_i^t \otimes h_j$ for $i, j = 1, 2, 3$ are obtained by convolving $h_{i,j}$ with a two-dimensional image X . The corresponding forward transform D will be a stack of nine block-circulant-circulant-block matrices. The tight-frame coefficients are given by the matrix-vector product $D\text{vec}(X)$, where $\text{vec}(X)$ denotes the vector obtained by concatenating the columns of X .

III. THE NUMERICAL ALGORITHM

The aim of this work is to provide a fast numerical scheme for solving the constrained problem in (3). By reformulating the problem (3) into some optimization problems with favorably separable structures, we notice that the problem (3) can be solved efficiently via the well-developed alternating direction method of multipliers (ADMM) for solving the constrained problem (3). Please see [7] and [8] for discussion.

As the proposed model is a convex optimization problem, there are efficient solvers for finding a global minimizer of (3). The solvers include the Bregman method [26], proximal splitting methods [27] and primal-dual methods [28], [29] Douglas-Rachford methods [30], and alternating direction of multiplier methods (ADMM). Here we just discuss the alternating direction method of multipliers. The other methods can also be applied and implemented.

We consider to recover z from f in the analysis based approach model (3). We assume that the set $\mathcal{Z} = \{z \in \mathbb{R}^n \mid \|z - \mu e\|_2^2 \leq \gamma\}$ is non-empty, which ensures that there exists a convex set of minimizers. Then we let $p = Df$,

Algorithm 1 Alternating Direction Method of Multipliers for Solving (7)

Input:	The maximal number of iterations ITER; The starting point $x^0 \in \text{dom}(f_1)$, $y^0 \in \text{dom}(f_2)$ and λ^0 ; the initial value of β
Output:	x^{ITER} which satisfies some stopping criterion
For	$k = 0$ to ITER - 1 do (k refers to the iteration index)
	Step 1. Find $x^{k+1} \in \text{argmin}_{z, f} (\lambda^k)^t (Qx + By^k) + \frac{\beta}{2} \ Qx + By^k\ ^2$
	Step 2. Find $y^{k+1} \in \text{argmin}_y f_2(y) + (\lambda^k)^t (Qx^{k+1} + By) + \frac{\beta}{2} \ Qx^{k+1} + By\ ^2$
	Step 3. $\lambda^{k+1} = \lambda^k + \beta(Qx^{k+1} + By^{k+1})$
Endfor	

$s = g \circ z$, $u = Af - s$. The model is rewritten as follows:

$$\begin{aligned} & \min_{z, f} \|u\|_1 + \alpha \|p\|_1, \\ & \text{subject to } z \in \mathcal{Z} \\ & \quad p = Df \\ & \quad u = Af - s \\ & \quad s = g \circ z \end{aligned} \quad (6)$$

in the model (6), let us define $\kappa(z)$ as

$$\kappa(z) = \begin{cases} 0, & \text{if } z \in \mathcal{Z}; \\ \infty, & \text{otherwise.} \end{cases}$$

Here we define

$$\begin{aligned} Q &= \begin{pmatrix} D & 0 \\ A & -I \\ 0 & I \end{pmatrix}, \quad B = \begin{pmatrix} -I & 0 & 0 \\ 0 & -I & 0 \\ 0 & 0 & -G \end{pmatrix} \\ x &= \begin{pmatrix} f \\ s \end{pmatrix}, \quad y = \begin{pmatrix} p \\ u \\ z \end{pmatrix}, \end{aligned}$$

where G is a diagonal matrix where its main diagonal entries are given by g , and $f_1(x) = 0$, $f_2(y) = \|u\|_1 + \alpha \|p\|_1 + \kappa(z)$. Thus the problem can be written as:

$$\begin{aligned} & \min_{z, f} f_2(y) \\ & \text{subject to } Qx + By = 0. \end{aligned} \quad (7)$$

The augmented Lagrangian of this problem writes:

$$L(x, y, \lambda) = f_2(y) + \lambda^t (Qx + By) + \frac{\beta}{2} \|Qx + By\|_2^2,$$

where λ are the Lagrangian multipliers given by three parts:

$$\lambda = \begin{pmatrix} \lambda_1 \\ \lambda_2 \\ \lambda_3 \end{pmatrix}.$$

Hence we derive the ADMM for solving (7) as presented in Algorithm 1.

Next we elaborate on the solutions of the subproblems of the ADMM method for (7). For the **Step 1**, we solve for the variable

$$x = \begin{pmatrix} f \\ s \end{pmatrix}$$

in the x -subproblem. Because $D^T D = I$, so the solution can be obtained by solving the normal equation as follows:

$$\begin{aligned} & \begin{pmatrix} I + A^T A & -A^T \\ -A & 2I \end{pmatrix} \begin{pmatrix} f^{k+1} \\ s^{k+1} \end{pmatrix} \\ &= \begin{pmatrix} D^T(p^k - \frac{\lambda_1^k}{\beta}) + A^T(u^k - \frac{\lambda_2^k}{\beta}) \\ -(u^k - \frac{\lambda_2^k}{\beta}) + (Gz^k - \frac{\lambda_3^k}{\beta}) \end{pmatrix}. \end{aligned} \quad (8)$$

When A is a blurring matrix generated by a symmetric point spread function, A can be diagonalized by a fast Fourier transform matrix Φ , i.e., $A = \Phi^T \Lambda \Phi$. Therefore we obtain the following decomposition:

$$\begin{aligned} & \begin{pmatrix} I + A^T A & -A^T \\ -A & 2I \end{pmatrix} \\ &= \begin{pmatrix} \Phi^T & 0 \\ 0 & \Phi^T \end{pmatrix} \begin{pmatrix} I + \Lambda^T \Lambda & -\Lambda^T \\ -\Lambda & 2I \end{pmatrix} \begin{pmatrix} \Phi & 0 \\ 0 & \Phi \end{pmatrix}, \end{aligned} \quad (9)$$

and the problem can be solved by using fast transforms.

For the **Step 2**, we solve for the variables

$$y = \begin{pmatrix} p \\ u \\ z \end{pmatrix}.$$

Since the variables p , u and z are decoupled, their optimal solutions can be calculated separately as follows: the p -subproblem is solved by

$$\begin{aligned} p^{k+1} &= \max \left\{ \left| (Df^{k+1} + \frac{\lambda_1^k}{\beta})_i \right| - \frac{\alpha}{\beta}, 0 \right\} \\ &\circ \text{sign} \left(Df^{k+1} + \frac{\lambda_1^k}{\beta} \right); \end{aligned} \quad (10)$$

the u -subproblem is solved by

$$\begin{aligned} u^{k+1} &= \max \left\{ \left| (Af^{k+1} - s^{k+1} + \frac{\lambda_2^k}{\beta})_i \right| - \frac{1}{\beta}, 0 \right\} \\ &\circ \text{sign} \left(Af^{k+1} - s^{k+1} + \frac{\lambda_2^k}{\beta} \right); \end{aligned} \quad (11)$$

the z -subproblem is given by

$$\begin{aligned} z^{k+1} &= \min_z \lambda_3^k (s^k - Gz) + \frac{\beta}{2} \|s^k - Gz\|_2^2 \\ &\text{subject to } z \in \mathcal{Z}, \end{aligned} \quad (12)$$

here the set $\mathcal{Z} = \{z \in \mathbb{R}^n \mid \|z - \mu e\|_2^2 \leq \gamma\}$. We can equivalently reformulate it as

$$\begin{aligned} z^{k+1} &= \min_z \frac{\beta}{2} \|s^k - Gz + \frac{\lambda_3^k}{\beta}\|_2^2 \\ &\text{subject to } z \in \mathcal{Z}. \end{aligned} \quad (13)$$

It is easy to show that the solution to (13) is given by

$$z^{k+1} = \mathcal{P}_{\mathcal{Z}} \left(\frac{\beta G s^k + G \lambda_3^k}{\beta G^T G} \right). \quad (14)$$

Here \mathcal{P} represents a projection (in Euclidean norm) onto the convex set \mathcal{Z} , see [37]. However, it has a closed-form expression and therefore turns to be an easy task to perform. The projection is simply given by the normalization of z

$$z^* = \begin{cases} z = \frac{\beta G s^k + G \lambda_3^k}{\beta G^T G}, & \text{if } \|z - \mu e\|_2^2 \leq \gamma \\ z / \|z - \mu e\|_2^2, & \text{otherwise.} \end{cases} \quad (15)$$

It can be computed explicitly and very accurately. Let us describe how to solve (14). Let $w = Gz$. The problem in (14) is written as follows:

$$\begin{aligned} \text{Find } w = \min_w \frac{\beta}{2} \|s^k - w + \frac{\lambda_3^k}{\beta}\|_2^2 \\ \text{subject to } w \in \mathbb{R}^n \end{aligned} \quad (16)$$

$$\|w - G\mu e\|_2^2 \leq \gamma. \quad (17)$$

For the constrained condition, when $z \in \mathcal{Z}$, it is the guarantee of $w \in \mathcal{Z}'$. where $\mathcal{Z}' = \{w \in \mathbb{R}^n \mid \|w - G\mu e\|_2^2 \leq \gamma\}$. Note that

$$\begin{aligned} \|w - G\mu e\|_2^2 &= \|Gz - G\mu e\|_2^2 \\ &\leq \|G\|_2^2 \|z - \mu e\|_2^2 \leq \|G\|_2^2 \gamma \leq \gamma. \end{aligned}$$

It is easy to show that the solution to (16) is given by

$$w = \mathcal{P}_{\mathcal{Z}'} \left(s^k + \frac{\lambda_3^k}{\beta} \right), \quad (18)$$

see [38] for the details. The projection is simply given by the normalization of w

$$w^* = \begin{cases} w = s^k + \frac{\lambda_3^k}{\beta}, & \text{if } \|z - \mu e\|_2^2 \leq \gamma \\ w / \|w - G\mu e\|_2^2, & \text{otherwise.} \end{cases} \quad (19)$$

Because $w = Gz$ and G is a diagonal matrix, the resulting solution can be given in (15).

For the **Step 3**, we just update the λ^{k+1} using the new values of the X^{k+1} and Y^{k+1} . The convergence of the method for the above convex objective function is guaranteed (see [7], [8]). In the Section IV, we present some numerical results to show the effectiveness of the proposed model.

A. Synthesis and Balanced Approaches

The matrix D in (3) can be considered to be an analysis operator. It can be viewed as analysis based approach [19]. Also we can formulate the multiplicative noise and blur removal problem by using synthesis and balanced based approaches in (20) and (21) respectively:

$$\begin{aligned} \min_{z, f} & \|g \circ z - AD^T d\|_1 + \alpha \|d\|_1, \\ \text{subject to } & \|z - \mu e\|_2^2 \leq \gamma. \end{aligned} \quad (20)$$

where $d = Df$.

$$\begin{aligned} \min_{z, f} & \|g \circ z - AD^T d\|_1 + \alpha_1 \|d\|_1 + \alpha_2 \|(I - DD^T)d\|_2^2, \\ \text{subject to } & \|z - \mu e\|_2^2 \leq \gamma. \end{aligned} \quad (21)$$

The synthesis based approach model (20) and the balanced based approach model (21) can be solved similarly as the

analysis based approach. In the synthesis based approach, we set $d = Df$, $p = D^T d$, $s = g \circ z$ and $u = Ap - s$ in (20). Now the model is rewritten as follows:

$$\begin{aligned} \min_{z, f} & \|u\|_1 + \alpha \|d\|_1, \\ \text{subject to } & z \in \mathcal{Z} \\ & p = D^T d \\ & s = g \circ z \\ & u = Ap - s \end{aligned} \quad (22)$$

we define

$$\begin{aligned} Q &= \begin{pmatrix} D^T & 0 \\ AD^T & -I \\ 0 & I \end{pmatrix}, \quad B = \begin{pmatrix} -I & 0 & 0 \\ 0 & -I & 0 \\ 0 & 0 & -G \end{pmatrix} \\ x &= \begin{pmatrix} d \\ s \\ z \end{pmatrix}, \quad y = \begin{pmatrix} p \\ u \\ z \end{pmatrix}, \end{aligned}$$

where G is a diagonal matrix where its main diagonal entries are given by g , and $f_1(x) = 0$, $f_2(y) = \|u\|_1 + \alpha \|d\|_1 + \kappa(z)$. We rewrite the problem similarly as the (7), also we can use the ADMM to solve it. For the **Step 1**, we solve for the variable

$$x = \begin{pmatrix} d \\ s \end{pmatrix}$$

in the subproblem. Because $D^T D = I$, so the solution can be obtained by solving the normal equation as follows:

$$\begin{aligned} & \begin{pmatrix} DD^T + DA^T AD^T & -DA^T \\ -AD^T & 2I \end{pmatrix} \begin{pmatrix} d^{k+1} \\ s^{k+1} \end{pmatrix} \\ &= \begin{pmatrix} D(p^k - \frac{\lambda_1^k}{\beta}) + DA^T(u^k - \frac{\lambda_2^k}{\beta}) \\ -(u^k - \frac{\lambda_2^k}{\beta}) + (Gz^k - \frac{\lambda_3^k}{\beta}) \end{pmatrix}. \end{aligned} \quad (23)$$

If we let

$$P = \begin{pmatrix} D & 0 \\ 0 & I \end{pmatrix},$$

$P^T P = I$, then the problem is:

$$\begin{aligned} & P \begin{pmatrix} I + A^T A & -A^T \\ -A & 2I \end{pmatrix} P^T \begin{pmatrix} d^{k+1} \\ s^{k+1} \end{pmatrix} \\ &= \begin{pmatrix} D(p^k - \frac{\lambda_1^k}{\beta}) + DA^T(u^k - \frac{\lambda_2^k}{\beta}) \\ -(u^k - \frac{\lambda_2^k}{\beta}) + (Gz^k - \frac{\lambda_3^k}{\beta}) \end{pmatrix}, \end{aligned}$$

let

$$y = P^T \begin{pmatrix} d^{k+1} \\ s^{k+1} \end{pmatrix},$$

at first we solve the problem

$$\begin{aligned} & \begin{pmatrix} I + A^T A & -A^T \\ -A & 2I \end{pmatrix} y \\ &= P^T \begin{pmatrix} D(p^k - \frac{\lambda_1^k}{\beta}) + DA^T(u^k - \frac{\lambda_2^k}{\beta}) \\ -(u^k - \frac{\lambda_2^k}{\beta}) + (Gz^k - \frac{\lambda_3^k}{\beta}) \end{pmatrix}. \end{aligned}$$



Fig. 1. The original images Parrot (left), Cameraman (middle) and Peppers (right).

the second step, we solve the problem:

$$P^T \begin{pmatrix} d^{k+1} \\ s^{k+1} \end{pmatrix} = y,$$

to find the solution.

For the **Step 2**, we solve for the variables

$$y = \begin{pmatrix} p \\ u \\ z \end{pmatrix}.$$

The variables p , u and z are decoupled, their optimal solutions can be calculated separately as follows: the p -subproblem is solved by

$$p^{k+1} = \frac{\lambda_1^k}{\beta} + D^T d^k;$$

the u -subproblem is solved by

$$\begin{aligned} u^{k+1} &= \max \left\{ \left| \left(AD^T d^{k+1} - s^{k+1} + \frac{\lambda_2^k}{\beta} \right)_i \right| - \frac{1}{\beta}, 0 \right\} \\ &\circ \text{sign} \left(AD^T d^{k+1} - s^{k+1} + \frac{\lambda_2^k}{\beta} \right); \end{aligned}$$

the z -subproblem is the same as the analysis based approach model (14).

The balanced based approach for (21) can be solved similarly. Now we let $d = Df$, $p = D^T d$, $s = g \circ z$, $u = Ap - s$ and $q = (I - DD^T)d$. The model can be written as follows:

$$\begin{aligned} \min_{z, f} \quad & ||u||_1 + \alpha_1 ||d||_1 + \alpha_2 ||q||_2^2 \\ \text{subject to } & z \in \mathcal{Z} \\ & p = D^T d \\ & s = g \circ z \\ & u = Ap - s \\ & q = (I - DD^T)d \end{aligned} \quad (24)$$

Using the ADMM method, at the **Step 1**, the subproblem is the same as the synthesis based approach in (23). At the **Step 2**, the p , u and z subproblem is the same as the synthesis based approach model. The q -subproblem is solved by

$$q^{k+1} = \frac{\lambda_4^k}{\beta} + (I - DD^T)d^k;$$

From the results, we know the solution of the balanced based approach in (20) is the same as the synthesis based approach in (21).

IV. EXPERIMENTAL RESULTS

In this section, we give numerical results on the image restoration for blurred images corrupted by multiplicative noise. We compare our results with those obtained by the CONVEX model proposed by Zhao *et al.* [18], the AA model proposed by Aubert and Aujol [1]. We remark in [18] that

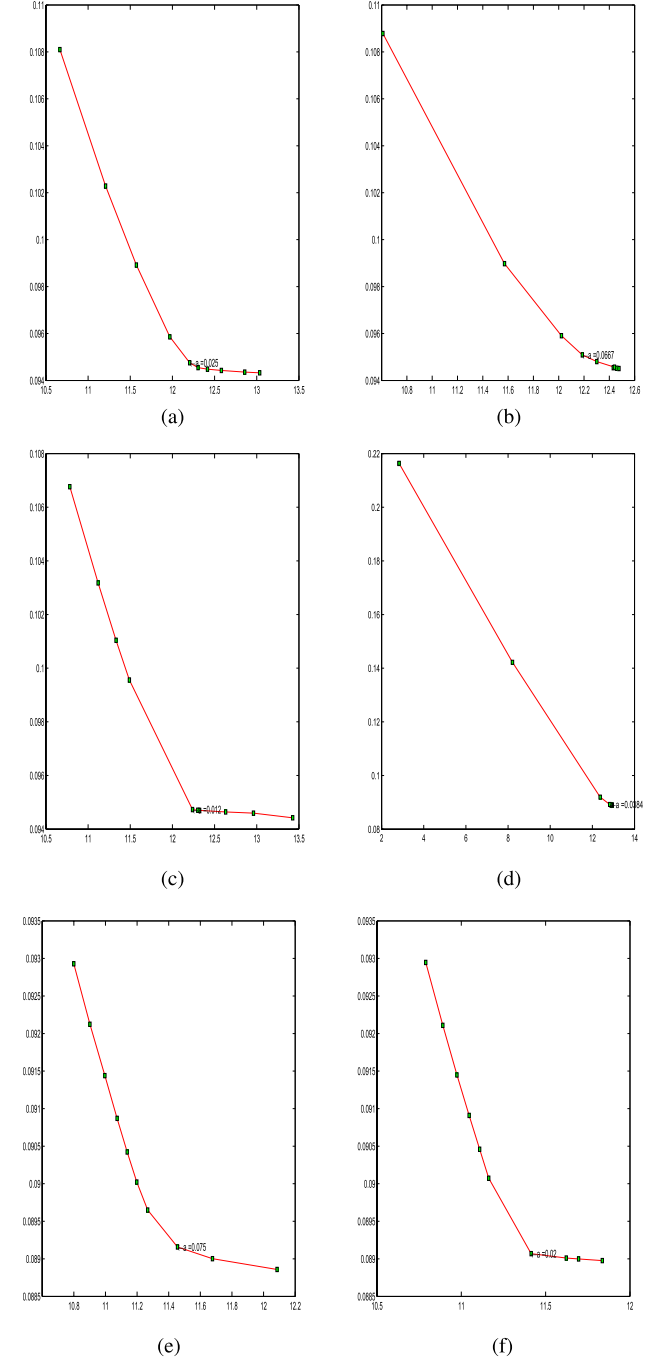


Fig. 2. The L-curves for the two images [Parrot or Pepper] with [Motion, Disk or Gaussian] blurs and multiplicative Gamma noise. (a) Parrot, Guassian blur and Gamma noise. $\gamma^* = 13.3$ and $\alpha = 0.025$. (b) Parrot, Motion blur and Gamma noise. $\gamma^* = 12.3$ and $\alpha = 0.0667$. (c) Parrot, Disk blur and Gamma noise. $\gamma^* = 12.5$ and $\alpha = 0.0120$. (d) Pepper, Guassian blur and Gamma noise. $\gamma^* = 17.7$ and $\alpha = 0.0384$. (e) Pepper, Motion blur and Gamma noise. $\gamma^* = 17.7$ and $\alpha = 0.0750$. (f) Pepper, Disk blur and Gamma noise. $\gamma^* = 17.7$ and $\alpha = 0.0200$.

it has been reported that the method is superior than the other existing methods. In the experiments, we make use of w used in [18] to employ the constraint in (3). Here the AA model can provide a baseline reference for the blur and multiplicative noise removal in the literature. In the two compared methods, the best restoration results are shown. All experiments were performed under MAC and Matlab R2013a

TABLE I
THE DEBLURRING RESULTS BY DIFFERENT MODELS

Images	Blurs	The Analysis Model					CONVEX Model			AA Model		
		PSNR	SSIM	Iter	Time-RC	Time-C	PSNR	SSIM	Time-C	PSNR	SSIM	Time-C
Pattor	Gaussian	24.48	0.64	114	822.84	27.98	23.87	0.69	4.65	23.32	0.61	12.37
	Motion	25.29	0.57	189	732.64	46.26	23.43	0.75	5.62	22.29	0.66	12.58
	Disk	25.24	0.58	117	878.38	29.51	23.55	0.44	12.34	21.71	0.56	11.80
Pepper	Gaussian	26.37	0.75	39	1502.02	30.23	25.55	0.65	26.18	24.81	0.71	53.53
	Motion	28.16	0.53	154	1254.84	117.61	26.61	0.74	34.81	25.99	0.72	53.18
	Disk	25.37	0.71	50	921.34	39.12	23.79	0.70	9.22	23.72	0.68	54.85

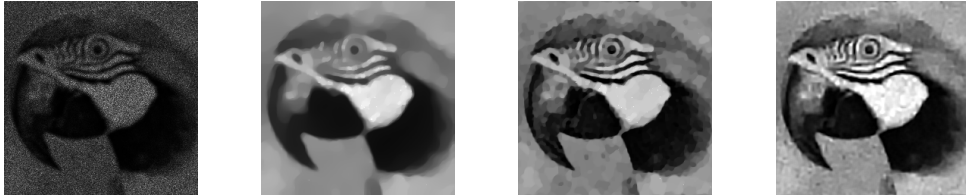


Fig. 3. The observed image corrupted by Gaussian blur and Gamma noise(subfigure 1). The result of AA model (subfigure 2) using $\alpha = 9 \times 10^{-2}$, the result of CONVEX model (subfigure 3) using $\alpha_2 = 1 \times 10^{-3}$, the result of the proposed model (subfigure 4) using $\alpha = 2.5 \times 10^{-2}$.



Fig. 4. The observed image corrupted by Motion blur and Gamma noise (subfigure 1). The result of AA model (subfigure 2) using $\alpha = 8 \times 10^{-2}$, the result of CONVEX model (subfigure 3) using $\alpha_2 = 8 \times 10^{-4}$, the result of the proposed model (subfigure 4) using $\alpha = 6.67 \times 10^{-2}$.

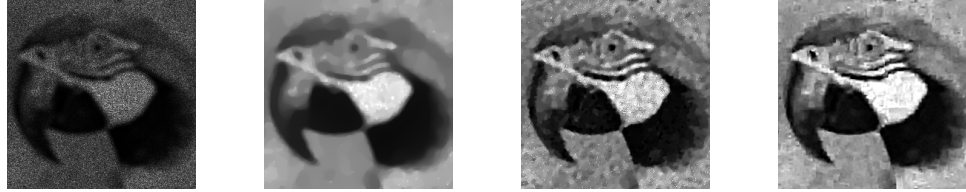


Fig. 5. The observed image corrupted by Disk blur and Gamma noise (subfigure 1). The result of AA model (subfigure 2) using $\alpha = 7 \times 10^{-2}$, the result of CONVEX model (subfigure 3) using $\alpha_2 = 4 \times 10^{-4}$, the result of the proposed model (subfigure 4) using $\alpha = 1.2 \times 10^{-2}$.

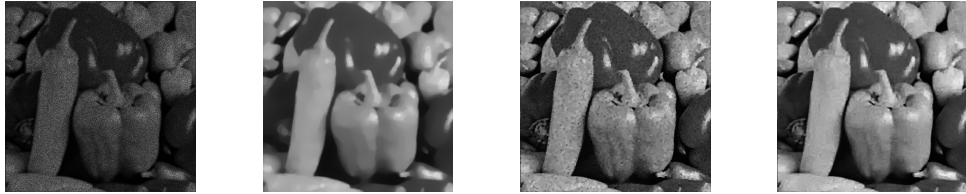


Fig. 6. The observed image corrupted by Gaussian blur and Gamma noise(subfigure 1). The result of AA model (subfigure 2) using $\alpha = 0.1$, the result of CONVEX model (subfigure 3) using $\alpha_2 = 6 \times 10^{-4}$, the result of the proposed model (subfigure 4) using $\alpha = 3.84 \times 10^{-2}$.

running on a desktop with an Intel Core i5 CPU 2.5GHz and 4GB 1600 MHz DDR3 of RAM memory.

The images “Parrot”, “Cameraman” and “Pepper” are tested in our experiment, see Figure 1. These testing images have been used and tested in [18]. The quality of the restored images is measured by PSNR (Peak Signal Noise Ratio) and SSIM (Structural Similarity Index) [31]. Suppose the image size is m -by- n , the PSNR value is defined as follows:

$$\text{PSNR} = 10 \log_{10} \left(\frac{V^2}{\text{MSE}} \right),$$

where $\text{MSE} = \sum_{i=1}^m \sum_{j=1}^n (\bar{x}(i, j) - x(x, j))^2 / (mn)$, x and \bar{x} are the original image and the recovered image respectively, and $V = \max_{i,j} |\bar{x}(i, j) - x(x, j)|$.

A. l_1 -Based L-Curve Method

In practice, we need to adjust the parameter α in order to get a better numerical performance and improve the convergence of the ADMM method. For the parameter α , we use the L-Curve tool [32], [33]. Here we plot for all valid regularization parameters associated with the norm $\|Dx_{\text{reg}}\|_1$

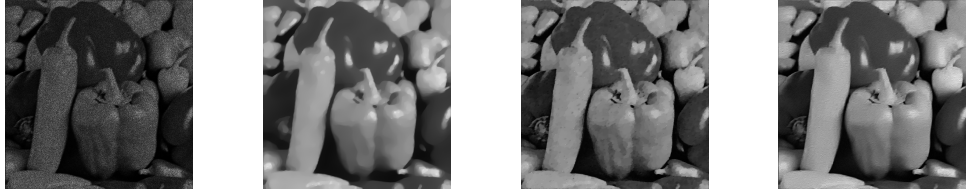


Fig. 7. The observed image corrupted by Motion blur and Gamma noise (subfigure 1). The result of AA model (subfigure 2) using $\alpha = 0.0975$, the result of CONVEX model (subfigure 3) using $\alpha_2 = 2 \times 10^{-3}$, the result of the proposed model (subfigure 4) using $\alpha = 7.5 \times 10^{-2}$.

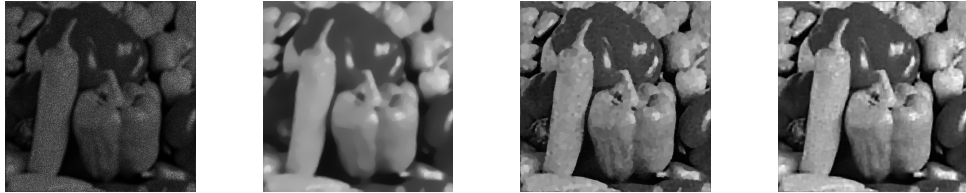


Fig. 8. The observed image corrupted by Disk blur and Gamma noise (subfigure 1). The result of AA model (subfigure 2) using $\alpha = 0.1$, the result of CONVEX model (subfigure 3) using $\alpha_2 = 6 \times 10^{-4}$, the result of the proposed model (subfigure 4) using $\alpha = 2 \times 10^{-2}$.

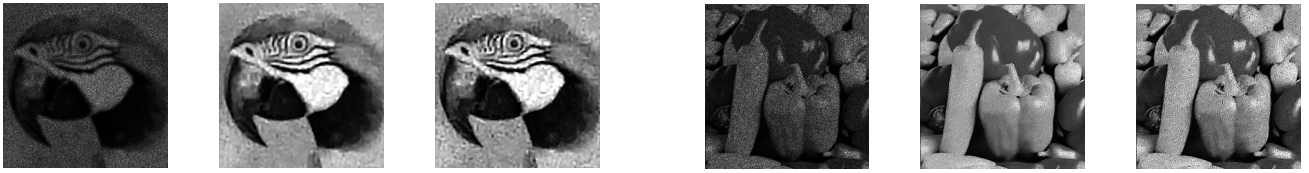


Fig. 9. The observed image corrupted by Gaussian blur and Gamma noise (Up-left figure). The result using γ^* (Up-middle figure). The result using $0.1 \times \gamma^*$ (Up-right figure). The result using $0.5 \times \gamma^*$ (Down-left figure). The result using $2 \times \gamma^*$ (Down-middle figure). The result using $5 \times \gamma^*$ (Down-right figure).

TABLE II
THE RESULTS USING DIFFERENT γ

	Parrot and Gaussian Blur			Pepper and Motion blur		
	PSNR	Iter	Time-C	PSNR	Iter	Time-C
γ^*	24.48	114	28.53	28.16	154	117.61
$0.1 \times \gamma^*$	24.94	200	49.13	26.81	242	100.48
$0.5 \times \gamma^*$	24.68	147	36.20	27.47	176	201.78
$2 \times \gamma^*$	17.40	36	9.06	21.91	45	36.17
$5 \times \gamma^*$	13.68	48	12.02	17.26	52	42.20

of the regularized solution and the corresponding residual norm $\|Fw - Hx_{\text{reg}}\|_1$.

This discrete ℓ_1 -based L-curve is a two-dimensional graph of the points

$$(\log \|Fw - Hx_\alpha\|_1, \log \|Dx_\alpha\|_1)$$

obtained by these regularization parameters α . In order to determine a reasonable regularization parameter, the best choice is to be the corner of the L-curve. It is used for the balance between the norm of the regularized solution and the residual norm. Here we refer to the reader [34], [35] for the corner detection in L-curve. In particular, we use the



Fig. 10. The observed image corrupted by Motion blur and Gamma noise (Up-left figure). The result using γ^* (Up-middle figure). The result using $0.1 \times \gamma^*$ (Up-right figure). The result using $0.5 \times \gamma^*$ (Down-left figure). The result using $2 \times \gamma^*$ (Down-middle figure). The result using $5 \times \gamma^*$ (Down-right figure).

method proposed by Hansen and O’Leary [36] for choosing the regularization parameter α , they defined the “corner” as the point on the L-curve with the maximal curvature. We employ the function (**l_corner** and **corner**) in the matlab package of Regularization Tools¹ proposed by Hansen to find the regularization parameter α , namely, such that the corresponding point on the L-curve lies on this corner [33]. For example, Figure 2 shows the figures of L-Curve for the experiment of different blur and Gamma noise, see Section IV-B. In the image, we take some points on the L-curve to compare the location of the “corner” point. In this experiment, we test our model for deblurring performance. In Figure 2(a), we show the L-curve graph of the Parrot degraded by Gaussian blur and Gamma noise case. We obtain the point $\alpha = 0.025$ as the regularization parameter which is the closest point of the corner in the L-curve. The other L-curve graphs are also shown in Figure 2 for the other testing cases. The regularization parameter can be computed automatically.

¹Regularization Tools Version 4.1, <http://www2.imm.dtu.dk/~pcha/Regutools/index.html>

TABLE III
THE COMPARISON FOR THE ANALYSIS AND SYNTHESIS METHODS

Images	Blurs	The Analysis Method				The Synthesis Method			
		PSNR	SSIM	Iter	Time-C	PSNR	SSIM	Iter	Time-C
peppers	Gaussian	26.37	0.75	39	43.38	25.55	0.76	78	108.69
	Motion	28.16	0.53	154	117.61	28.22	0.41	244	353.72
	Disk	25.37	0.71	50	39.12	24.69	0.74	55	85.17

TABLE IV
THE DENOISING RESULTS BY DIFFERENT MODELS

Images	Noise	The Analysis Model					CONVEX Model				AA Model			
		PSNR	SSIM	Iter	Time-RC	Time-C	PSNR	SSIM	Iter	Time-C	Psnr	SSIM	Iter	Time-C
Cameraman	Gaussian	29.14	0.76	54	1118.48	13.56	27.33	0.80	468	9.18	25.01	0.73	800	4.52
	Gamma	28.18	0.58	172	1464.95	42.85	26.64	0.55	1000	19.54	26.28	0.70	800	4.44
	Rayleigh	23.54	0.69	60	2289.71	14.75	21.60	0.68	70	1.52	21.26	0.64	1000	6.89
Parrot	Gaussian	28.56	0.74	46	2334.06	11.21	27.44	0.83	469	8.97	25.84	0.74	620	4.31
	Gamma	28.63	0.75	86	1611.82	20.95	27.53	0.71	707	13.82	24.56	0.68	1000	6.76
	Rayleigh	27.20	0.66	60	2308.85	16.38	23.49	0.65	800	15.60	22.11	0.61	650	16.15



Fig. 11. The observed image corrupted by Gaussian noise (subfigure 1). The result of AA model (subfigure 2) using $\alpha = 0.07$, the result of CONVEX model (subfigure 3) using $\alpha_2 = 8 \times 10^{-4}$, the result of our model (subfigure 4) using $\alpha = 1 \times 10^{-4}$.



Fig. 12. The observed image corrupted by Gamma noise (subfigure 1). The result of AA model (subfigure 2) using $\alpha = 0.06$, the result of CONVEX model (subfigure 3) using $\alpha_2 = 7 \times 10^{-4}$, the result of our model (subfigure 4) using $\alpha = 2 \times 10^{-5}$.

B. Image Deblurring

In this experiment, we test the performance of the analysis based approach model (3) for image deblurring. We test three kinds of blurs: Gaussian blur, Motion blur and Disk blur. The Matlab commands are `fspecial('motion', 5,30)`, `fspecial('gaussian', [7, 7], 2)` and `fspecial('disk', 5)`. The blurred images are contaminated by multiplicative Gamma noise with mean 1 and $L = 10$. In Table I, we show the PSNR values, iterations and the computational time of the restored images by different methods. Each entry of the table refers to a number by taking the average results of ten noise cases under the same experimental setting (type of blur and level of noise). Here iteration number is rounded up to the integer and computational time is rounded up to the second. In the table, the ‘‘Time-RC’’ column includes all the calculation time by determining the regularization parameter from the L-curve and restoring an image. the ‘‘Time-C’’ column refers to the image restoration by assuming that a suitable regularization parameter is already chosen. We see the performance of the proposed model performs quite well in terms of PSNR values.

The SSIM results of the proposed model may not be always the best compared with the CONVEX model and the AA model. Here we make use of ℓ_1 -based L-curve to select the regularization parameter automatically based on the residual and smoothness of the computed solution. It is not necessary to choose regularization parameters for good SSIM values. However, the PSNR results of the proposed model are always better than those of the other methods. Experimental results show that these regularization parameters can provide large PSNR values. In Figures 3-8, we display the restored images by using the CONVEX model and the AA model. In the two models, the suitable regularization parameters have obtained, we report their computational time (in second) for image restoration only. It is clear from the figures that the restoration results of our model are still visually better than those by the CONVEX model and the AA model.

C. The Effect of γ

In this experiment, we study the effect of γ in the deblurring model by using the analysis approach in (3)). We use the



Fig. 13. The observed image corrupted by Rayleigh noise (subfigure 1). The result of AA model (subfigure 2) using $\alpha = 0.13$, the result of CONVEX model (subfigure 3) using $\alpha_2 = 8.5 \times 10^{-3}$, the result of our model (subfigure 4) using $\alpha = 1 \times 10^{-4}$.



Fig. 14. The observed image corrupted by Gaussian noise (subfigure 1). The result of AA model (subfigure 2) using $\alpha = 0.07$, the result of CONVEX model (subfigure 3) using $\alpha_2 = 8 \times 10^{-4}$, the result of our model (subfigure 4) using $\alpha = 1 \times 10^{-3}$.

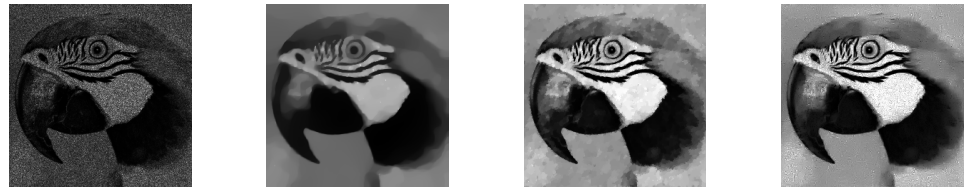


Fig. 15. The observed image corrupted by Gamma noise (subfigure 1). The result of AA model (subfigure 2) using $\alpha = 0.08$, the result of CONVEX model (subfigure 3) using $\alpha_2 = 8 \times 10^{-4}$, the result of our model (subfigure 4) using $\alpha = 4 \times 10^{-4}$.

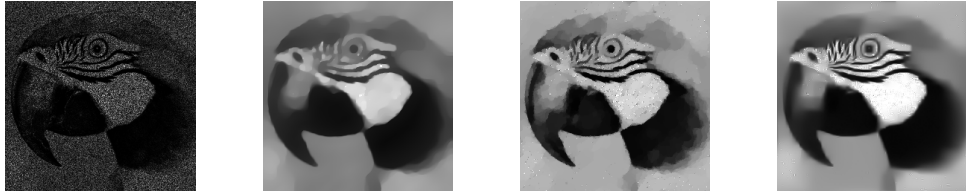


Fig. 16. The observed image corrupted by Rayleigh noise (subfigure 1). The result of AA model (subfigure 2) using $\alpha = 0.2$, the result of CONVEX model (subfigure 3) using $\alpha_2 = 6 \times 10^{-3}$, the result of our model (subfigure 4) using $\alpha = 1 \times 10^{-4}$.

examples in Section IV-B (Experiment 1: Parrot and Gaussian blur, Experiment 2: Pepper and Motion blur) to compare deblurring results by using γ^* , $0.1 \times \gamma^*$, $0.5 \times \gamma^*$, $2 \times \gamma^*$, $5 \times \gamma^*$ based on the values of γ^* in Figures 2(a) and 2(e) respectively. The deblurring results in PSNR are given in Table II. And the deblurred images are displayed in Figure 9 and Figure 10. According to the table, we see that when the parameter is less than γ^* , the deblurring results are not affected too much. However, when the parameter is larger than γ^* , the deblurring results are not good. It is clear that the constraint $\|z - \mu e\|_2^2 \leq \gamma$ is too relaxed, and therefore the deblurring quality cannot be controlled.

D. The Analysis and Synthesis Methods

In this subsection, we test the performance of the analysis method in (3) and the synthesis method in (20). In the experiment, we test three kinds of blurs, namely motion blur, Gaussian blur and Disk blur. Their Matlab commands are:

`fspecial('motion',5,30)` `fspecial('gaussian', [7, 7], 2)` and `fspecial('disk', 5)`. The blurred image are contaminated by multiplicative Gamma noise with mean 1 and $L = 10$. The deblurring results in PSNR and SSIM are given in Table III. Here ℓ_1 -based L-curve is used to select regularization parameters in both analysis and synthesis approaches. The results show that the restoration results by using the analysis method are slightly better than those by using the synthesis method.

E. Image Denoising

In this experiment, we test the performance of the analysis based approach model (3) of three types of multiplicative noise (Gaussian, Gamma and Rayleigh noise). The Gaussian noise is generated by the Matlab build-in function “randn”. The Gamma noise is generated by the Matlab build-in function “gammrnd”. The Rayleigh noise is generated by $\theta \sqrt{-2 \log(1 - u)}$, where u is a uniformly distributed random variable generated by the Matlab build-in function “rand”.

The mean of these noises are set to be 1, and variance are 0.04, 0.1 and 0.2732 respectively. Table IV shows the PSNR values, iterations and the computational time (in seconds) of the restored images by different methods. We notice that each entry of the table refers to a number by taking the average results of ten noise cases under the same experimental setting (type of noise and level of noise). Figures 11-16 show the denoising images by using different models of the experiment. It is clear from the table and the figures that the restoration results of our model are visually better than those by the CONVEX model and the AA model.

V. CONCLUDING REMARKS

In this paper, we have proposed a constrained convex variational model for recovering blurred images corrupted by multiplicative noise of different types. In the model, we studied the functional by minimizing two variables: the restored image and the noise image on the l_1 data-fitting term, the variance term, and the tight-frame term. We developed an efficient alternating direction method for solving the proposed model. In the experiments, we use the idea of L-curve by considering the points generated by the two terms, and determine the regularization parameter based on the maximal change of the curve. Extensive numerical experiments are provided to illustrate the state-of-the-art performance of the proposed model.

REFERENCES

- [1] G. Aubert and J.-F. Aujol, "A variational approach to removing multiplicative noise," *SIAM J. Appl. Math.*, vol. 68, no. 4, pp. 925–946, 2008.
- [2] S. Durand, J. Fadili, and M. Nikolova, "Multiplicative noise removal using L_1 fidelity on frame coefficients," *J. Math. Imag. Vis.*, vol. 36, no. 3, pp. 201–226, 2010.
- [3] Y.-M. Huang, M. K. Ng, and Y.-W. Wen, "A new total variation method for multiplicative noise removal," *SIAM J. Imag. Sci.*, vol. 2, no. 1, pp. 20–40, 2009.
- [4] F. Li, M. K. Ng, and C. Shen, "Multiplicative noise removal with spatially varying regularization parameters," *SIAM J. Imag. Sci.*, vol. 3, no. 1, pp. 1–20, 2010.
- [5] D. Yin, Y. Gu, and P. Xue, "Speckle-constrained variational methods for image restoration in optical coherence tomography," *J. Opt. Soc. Amer. A*, vol. 30, no. 5, pp. 878–885, 2013.
- [6] A. Tekalp and G. Pavlovic, "Restoration of scanned photographic images," in *Digital Image Restoration*, A. K. Katsaggelos, Ed. Berlin, Germany: Springer-Verlag, 1991, pp. 209–239.
- [7] M. K. Ng, P. Weiss, and X. Yuan, "Solving constrained total-variation image restoration and reconstruction problems via alternating direction methods," *SIAM J. Sci. Comput.*, vol. 32, no. 5, pp. 2710–2736, 2010.
- [8] M. K. Ng, F. Wang, and X. Yuan, "Inexact alternating direction methods for image recovery," *SIAM J. Sci. Comput.*, vol. 33, no. 4, pp. 1643–1668, 2011.
- [9] L. Rudin, P.-L. Lions, and S. Osher, "Multiplicative denoising and deblurring: Theory and algorithms," in *Geometric Level Set Methods in Imaging, Vision, and Graphics*. New York, NY, USA: Springer-Verlag, 2003, pp. 103–119.
- [10] J. Shi and S. Osher, "A nonlinear inverse scale space method for a convex multiplicative noise model," *SIAM J. Imag. Sci.*, vol. 1, no. 3, pp. 294–321, 2008.
- [11] M. Tur, K. C. Chin, and J. W. Goodman, "When is speckle noise multiplicative?" *Appl. Opt.*, vol. 21, no. 7, pp. 1157–1159, 1982.
- [12] R. F. Wagner, S. W. Smith, J. M. Sandrik, and H. Lopez, "Statistics of speckle in ultrasound B-scans," *IEEE Trans. Sonics Ultrason.*, vol. 30, no. 3, pp. 156–163, May 1983.
- [13] Y. M. Huang, L. Moisan, M. K. Ng, and T. Zeng, "Multiplicative noise removal via a learned dictionary," *IEEE Trans. Image Process.*, vol. 21, no. 11, pp. 4534–4543, Nov. 2012.
- [14] T. Teuber and A. Lang, "Nonlocal filters for removing multiplicative noise," in *Scale Space and Variational Methods in Computer Vision*. Heidelberg, Germany: Springer-Verlag, 2012, pp. 50–61.
- [15] Y. Huang, T. Zeng, and M. Ng, "The convex relaxation method on deconvolution model with multiplicative noise," *Commun. Comput. Phys.*, vol. 13, no. 4, pp. 1066–1092, 2013.
- [16] F. Wang and M. K. Ng, "A fast minimization method for blur and multiplicative noise removal," *Int. J. Comput. Math.*, vol. 90, pp. 48–61, 2013.
- [17] Y. Dong and T. Zeng, "A convex variational model for restoring blurred images with multiplicative noise," *SIAM J. Imag. Sci.*, vol. 6, no. 3, pp. 1598–1625, 2013.
- [18] X.-L. Zhao, F. Wang, and M. K. Ng, "A new convex optimization model for multiplicative noise and blur removal," *SIAM J. Imag. Sci.*, vol. 7, no. 1, pp. 456–475, 2014.
- [19] J.-F. Cai, R. H. Chan, L. Shen, and Z. Shen, "Simultaneously inpainting in image and transformed domains," *Numer. Math.*, vol. 4, no. 112, pp. 509–533, 2009.
- [20] J.-F. Cai, R. Chan, L. Shen, and Z. Shen, "Restoration of chopped and nodded images by framelets," *SIAM J. Sci. Comput.*, vol. 30, no. 3, pp. 1205–1227, 2008.
- [21] J.-F. Cai, R. H. Chan, L. Shen, and Z. Shen, "Convergence analysis of tight framelet approach for missing data recovery," *Adv. Comput. Math.*, vol. 31, no. 1, pp. 87–113, 2009.
- [22] J.-F. Cai, R. H. Chan, and Z. Shen, "A framelet-based image inpainting algorithm," *Appl. Comput. Harmon. Anal.*, vol. 24, no. 2, pp. 131–149, Mar. 2008.
- [23] R. H. Chan, T. F. Chan, L. Shen, and Z. Shen, "Wavelet algorithms for high-resolution image reconstruction," *SIAM J. Sci. Comput.*, vol. 24, no. 4, pp. 1408–1432, 2003.
- [24] A. Ron and Z. Shen, "Affine systems in $L_2(\mathbb{R}^d)$: The analysis of the analysis operator," *J. Funct. Anal.*, vol. 148, no. 2, pp. 408–447, 1997.
- [25] B. Dong and Z. Shen, "MRA based wavelet frames and applications," Univ. California Los Angeles, Los Angeles, CA, USA, CAM Rep., 2010. [Online]. Available: <ftp://ftp.math.ucla.edu/pub/camreport/cam1069.pdf>
- [26] T. Goldstein and S. Osher, "The split Bregman method for L_1 -regularized problems," *SIAM J. Imag. Sci.*, vol. 2, no. 2, pp. 323–343, 2009.
- [27] P. L. Combettes and J.-C. Pesquet, "Proximal splitting methods in signal processing," in *Fixed-Point Algorithms for Inverse Problems in Science and Engineering*. New York, NY, USA: Springer-Verlag, 2011, pp. 185–212.
- [28] A. Chambolle and T. Pock, "A first-order primal-dual algorithm for convex problems with applications to imaging," *J. Math. Imag. Vis.*, vol. 40, no. 1, pp. 120–145, 2011.
- [29] E. Esser, X. Zhang, and T. F. Chan, "A general framework for a class of first order primal-dual algorithms for convex optimization in imaging science," *SIAM J. Imag. Sci.*, vol. 3, no. 4, pp. 1015–1046, 2010.
- [30] P. L. Combettes and V. R. Wajs, "Signal recovery by proximal forward-backward splitting," *Multiscale Model. Simul.*, vol. 4, no. 4, pp. 1168–1200, 2005.
- [31] Z. Wang, A. C. Bovik, H. R. Sheikh, and E. P. Simoncelli, "Image quality assessment: From error visibility to structural similarity," *IEEE Trans. Image Process.*, vol. 13, no. 4, pp. 600–612, Apr. 2004.
- [32] P. C. Hansen, "The L-curve and its use in the numerical treatment of inverse problems," IMM, Dept. Math. Model., Tech. Univ. Denmark, Kongens Lyngby, Denmark, 1999.
- [33] P. C. Hansen, "Analysis of discrete ill-posed problems by means of the L-curve," *SIAM Rev.*, vol. 34, no. 4, pp. 561–580, Dec. 1992.
- [34] J. L. Castellanos, S. Gómez, and V. Guerra, "The triangle method for finding the corner of the L-curve," *Appl. Numer. Math.*, vol. 43, no. 4, pp. 359–373, 2002.
- [35] P. C. Hansen, "Deconvolution and regularization with Toeplitz matrices," *Numer. Algorithms*, vol. 29, no. 4, pp. 323–378, 2002.
- [36] P. C. Hansen and D. P. O'Leary, "The use of the L-curve in the regularization of discrete ill-posed problems," *SIAM J. Sci. Comput.*, vol. 14, no. 6, pp. 1487–1503, 1993.
- [37] P. Weiss, L. Blanc-Féraud, and G. Aubert, "Efficient schemes for total variation minimization under constraints in image processing," *SIAM J. Sci. Comput.*, vol. 31, no. 3, pp. 2047–2080, 2009.
- [38] W. Deng, W. Yin, and Y. Zhang, "Group sparse optimization by alternating direction method," Dept. Comput. Appl. Math., Rice Univ., Houston, TX, USA, Tech. Rep. TR11-06, 2011.



Fan Wang received the B.Sc. and M.Phil. degrees from Lanzhou University, Lanzhou, China, in 2001 and 2004, respectively, and the Ph.D. degree from Hong Kong Baptist University, in 2012. He is currently a Lecturer with the Department of Mathematics and Statistics, Lanzhou University. He joined the Institute for Computational Mathematics, Hong Kong Baptist University in 2009. His research interests include image processing, scientific computing, and data mining.



Xi-Le Zhao received the M.S. and Ph.D. degrees from the University of Electronic Science and Technology of China (UESTC), Chengdu, China, in 2009 and 2012, respectively. He is currently an Associate Professor with the School of Mathematical Sciences, UESTC. His main research interests are focused numerical linear algebra and sparse optimization.



Michael K. Ng received the B.Sc. and M.Phil. degrees from the University of Hong Kong, in 1990 and 1992, respectively, and the Ph.D. degree from the Chinese University of Hong Kong in 1995. He is currently a Chair Professor with the Department of Mathematics, Hong Kong Baptist University. He joined Hong Kong Baptist University. He was a Research Fellow of Computer Sciences Laboratory with Australian National University from 1995 to 1997, and an Assistant/ an Associate Professor with the University of Hong Kong from 1997 to 2005. His research interests include bioinformatics, image processing, scientific computing and data mining, and he serves on the editorial boards of international journals.